Stacking-dependent energetics and electronic structure of ultrathin polymorphic V_2VI_3 topological insulator nanofilms

Can Li,[1,2,*] Torben Winzer,[1,*] Aron Walsh,[3,1] Binghai Yan,[4,5] Catherine Stampfl,[6,1] and Aloysius Soon[1,†]

[1]*Global E3 Institute, Department of Materials Science and Engineering, Yonsei University, Seoul, Korea*

[2]*Department of Materials Science and Engineering, China Jiliang University, Zhejiang, China*

[3]*Centre for Sustainable Chemical Technologies, Department of Chemistry, University of Bath, Bath, United Kingdom*

[4]*Max Planck Institute for Chemical Physics of Solids, NöthnitzerStr. 40, 01187 Dresden, Germany*

[5]*Max Planck Institute for Physics of Complex Systems, NöthnitzerStr. 38, 01187 Dresden, Germany*

[6]*School of Physics, University of Sydney, NSW 2006, Australia*

(Received 24 June 2014; published 29 August 2014)

Topological insulators represent a paradigm shift in surface physics. The most extensively studied Bi_2Se_3-type topological insulators exhibit layered structures, wherein neighboring layers are weakly bonded by van der Waals interactions. Using first-principles density-functional theory calculations, we investigate the impact of the stacking sequence on the energetics and band structure properties of three polymorphs of Bi_2Se_3, Bi_2Te_3, and Sb_2Te_3. Considering their ultrathin films up to 6 nm as a function of its layer thickness, the overall dispersion of the band structure is found to be insensitive to the stacking sequence, while the band gap is highly sensitive, which may also affect the critical thickness for the onset of the topologically nontrivial phase. Our calculations are consistent with both experimental and theoretical results, where available. We further investigate tribological layer slippage, where we find a relatively low energy barrier between two of the considered structures. Both the stacking-dependent band gap and low slippage energy barriers suggest that polymorphic stacking modification may offer an alternative route for controlling the properties of this new state of matter.

DOI: 10.1103/PhysRevB.90.075438 PACS number(s): 71.20.−b, 73.20.At, 73.43.Nq, 75.70.Tj

Topological insulators (TIs) have remarkable electronic properties since the role of relativistic interactions [e.g., spin-orbit coupling (SOC)] is fundamentally different from conventional insulators and semiconductors [1–4]. TIs combine an insulating band gap in the bulk of the material with conductive surface states that are protected by time-reversal symmetry [5,6]. The topological behavior has been theoretically predicted and experimentally observed in a variety of systems [7] such as HgTe quantum wells [1], the Bi_2Se_3 family of compounds [8–11], Heusler compounds [12–14], pyrochlores [15], Kondo insulators [16], and thallium-based ternary chalcogenides [17]. Aside from the fundamental research in condensed matter physics, TIs have great potential to impact multiple areas of application (e.g., electronic, optoelectronic, and spintronic materials, thermoelectric materials, phase-change memory, and catalytic chemistry) [18,19].

To effectively explore the surface conductivity of TIs, ultrathin films with a large surface-to-volume ratio provide attractive systems for transport studies, which are highly relevant for electronic device applications [18]. For this purpose, the V_2VI_3 compounds Bi_2Se_3, Bi_2Te_3, and Sb_2Te_3 are a good choice owing to their layered rhombohedral crystal structure with space group *R-3m*. The structure contains five atomic layers as a basic unit, denoted as a quintuple layer (QL). There is strong chemical bonding within a QL, with weak van der Waals (vdW) interactions between different QLs. V_2VI_3 compounds can be easily grown as two-dimensional thin films by molecular beam epitaxy [10,20]. The two-dimensional nanostructures of Bi_2Se_3, Bi_2Te_3, and Sb_2Te_3 have been researched both theoretically and experimentally [9,21–23]. Their electronic structure depends on the thickness of the film: Above a critical thickness (D), films will transform from a normal insulator (NI) to a TI [22]. For the Bi_2Se_3 system, $D =$ 6 QL (about 6 nm) [21,24], while $D =$ 2 or 3 QL (about 2 or 3 nm) for Bi_2Te_3 [9,24,25] and 4 QL (about 4 nm) for Sb_2Te_3 [23]. Below the critical thickness, a surface band gap opens, due to hybridization of overlapping surface-state wave functions [21]. Thus, a minimum film thickness is suggested for topological electronic device applications.

Although the critical thicknesses of Bi_2Se_3, Bi_2Te_3, and Sb_2Te_3 have been studied in theory and experiment, the effect of pressure and stress, which are critical factors in real environments, have not been clearly explored [26–28]. Liu *et al.* have indicated that uniaxial strain in the ⟨111⟩ direction is an important parameter for influencing the topological insulating phase and the direct band gap of Bi_2Se_3 at the Γ point [22,26]. However, aside from uniaxial strain, shear strain could also be important in applications for ultrathin layered material: such as graphite [29], boron nitride [30], and V_2VI_3 compounds. The weak van der Waals force between these layers leads to the possibility of layer slippage and polytypism. When layered materials are used as mechanical components of nanodevices, the properties of friction are extremely important. The nanotribologies of bilayer graphene and boron nitride layers have been intensively researched; the results show that the associated energy barriers are extremely low [29–31]. The influence of layer sequencing and slippage in V_2VI_3 TI compounds, which directly relates to their usage in electronic device applications, is the subject of this study.

In these V_2VI_3 compounds, there are three QLs in each bulk conventional hexagonal unit cell, as shown in Fig. 1. There are also three unique lattice sites (A, B, and C). Different

*These authors contributed equally to this work.

†Corresponding author: aloysius.soon@yonsei.ac.kr

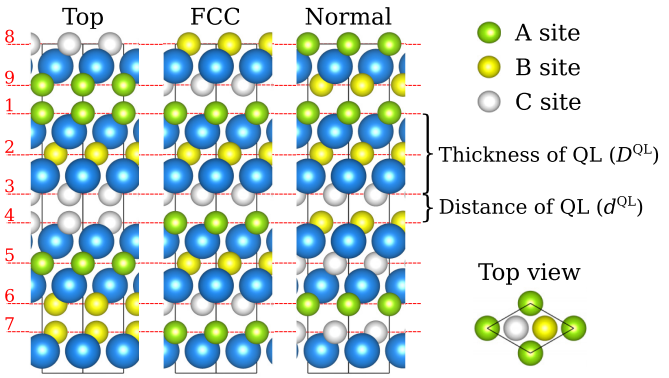

FIG. 1. (Color online) The atomic structures of V_2VI_3 polymorphs: the *top* (ABC-CAB-BCA), *fcc* (ABC-ABC-ABC), and *normal* (ABC-BCA-CAB) stacking sequences. Large spheres (blue) are used to represent the group-V atoms, while the small ones (green, yellow, and white) for group-VI atoms. The stacking sequence is labeled by the group-VI atomic layer according to the numbers (given in red).

polymorphic stacking types are labeled by the group-VI atoms in each QL. Thus, the *normal* structure has an ABC-BCA-CAB stacking sequence, whereas the ABC-CAB-BCA *top* like stacking (e.g., A-on-A, C-on-C, etc.) is denoted as the *top* structure and an ABC-ABC-ABC *fcc*-like stacking will then correspond to the *fcc* structure. Due to the weak interaction between these QLs and the strong covalent bonding within each QL, when a shear stress is applied perpendicular to the z direction, inter-QLs could easily move or experience a mechanical slip. X-ray diffraction experiments for V_2VI_3 compounds confirm the existence of the *normal* structure, while the other polymorphic *fcc* and *top* structures have not yet been experimentally determined. However, if formed predominately near/at the surface, alternative polymorphic stacking sequences may not give rise to an appreciable difference in their diffraction patterns.

In this paper, we employ density-functional theory (DFT) calculations (with SOC treated explicitly) to study the effects of polymorphic stacking and planar slippage on the electronic structures and the critical thickness of the polymorphs of V_2VI_3 (namely, Bi_2Se_3, Bi_2Te_3, and Sb_2Te_3) ultrathin nanofilms as a function of film thickness.

I. METHODOLOGY AND COMPUTATIONAL APPROACH

All DFT calculations, including geometry relaxation and electronic structure, are performed on the basis of the projector augmented wave method [32] implemented in the Vienna *ab initio* simulation package (VASP) code [33]. The exchange-correlation functional used is the generalized gradient approximation (GGA) due to Perdew, Burke, and Ernzerhof (PBE) [34,35], including scalar-relativistic effects in addition to SOC. The latter is known to be of great importance in accounting for the topologically protected surface states in TIs. The kinetic energy cutoff of electron wave functions is set to 500 eV and a **k**-point sampling of $12\times12\times1$ for all films was found to be converged. A vacuum region of 20 Å is used to avoid spurious interactions between repeating slabs. Both the shape and size of the unit cell and the relative atomic positions are relaxed with a force tolerance of 0.01 eV/Å. The dispersion-corrected DFT approach due to Grimme *et al.* (DFT + D2) has been used in which long-range dispersion interactions are empirically described by a pair potential of the C_6/R_0 form [36]. The Grimme-D2 coefficients are obtained from values tabulated in terms of the chemical identity of the atoms: $C_6 =$ 63.565, 38.459, 12.643, and 31.750; $R_0 =$ 1.725, 1.710, 1.610, and 1.720 for Bi, Sb, Se, and Te atoms, respectively [37].

In addition, hybrid DFT calculations at the level of HSE06+SOC for Bi_2Se_3 nanofilms have been used to study the electronic band structure. This is because the HSE06 hybrid functional typically presents a considerable improvement over semilocal density functionals for the description of the band gaps of solid-state systems [38,39]. This, in turn, is compared to available results using the van der Waals density functional with Cooper's exchange (vdW-DF$_x^{C09}$) [40] and GW [41] calculations in the literature.

The QL-QL interaction energies of ultrathin nanofilms E^{QL} from 1 QL to 6 QLs have been calculated using

$$E^{QL} = \frac{E^{sys} - N^{QL}E^{1QL}}{N^{QL}}, \tag{1}$$

where E^{sys} and E^{1QL} are the total energy of the system in question and that of 1 QL, respectively, and N^{QL} is the number of QLs in that system. Since the base unit is 1 QL, E^{QL} denotes the relative thermodynamic stability of the ultrathin film stacked per QL. In addition, to investigate the planar slippage energy barriers for these V_2VI_3 polymorphs, we employ the climbing-image nudged elastic band (CI-NEB) method at the level of PBE+D2 [42].

II. RESULTS AND DISCUSSION

A. Bulk structures of V_2VI_3 compounds

The crystal structures for three different polymorphic stacking sequences, *normal*, *fcc*, and *top*, are shown in Fig. 1, with the optimized lattice constants listed in Table I. The DFT + D2 optimized bulk structures are found to be in good agreement with the available experimental results [43] and the vdW-DF$_x^{C09}$ values [40], and are much closer to these results than previously calculated theoretical results (which do not include vdW corrections) [44]. This signals that the DFT+D2 approach is adequate for describing these weakly bonded layered systems. Cohesive energies of the bulk V_2VI_3 polymorphs are calculated and we find that all bulk structures yield a negative value, i.e., stable with respect to their corresponding atomic energies (see Table I). The *normal* structure is the most favored bulk polymorph, while the *top* structure is least stable. However, for Bi_2Te_3 and Sb_2Te_3 the differences between *normal*, *fcc*, and *top* structures are marginal. Only the *normal* stacking of Bi_2Se_3 is notably more stable compared to the other polymorphs. We have calculated the electronic band structures of bulk *normal* Bi_2Se_3 with PBE+SOC and HSE+SOC. The band-gap energy E_g of bulk Bi_2Se_3 is calculated to be 0.36 eV for PBE+SOC and 0.28 eV for HSE06+SOC, respectively. Surprisingly, the PBE+SOC E_g seems to be in a better agreement with other theoretical reports (0.30 eV) and experimental data (0.35 eV) than the

TABLE I. Lattice constants, electronic band gap, and cohesive energy of bulk V_2VI_3 compounds. The lattice constants a and c and cohesive energy E_{coh} are calculated using PBE+D2+SOC and are reported in Å and eV, respectively. The electronic band gap E_g is in eV and is calculated using PBE+SOC (the HSE06+SOC derived E_g for Bi_2Se_3 is 0.28 eV). Our results are compared to available experimental and theoretical values in the literature. The van der Waals density functional with Cooper's exchange (vdW-DF_x^{C09}) was used in Ref. [40].

		Bi_2Se_3	Bi_2Te_3	Sb_2Te_3
	normal	4.092	4.349	4.195
	fcc	4.071	4.290	4.144
a	*top*	4.057	4.282	4.142
	Experiment	4.138[a]	4.383[a]	4.250[a]
	Theory (*normal*)	4.125[b]	4.360[b], 4.530[c]	4.440[c]
	normal	28.91	31.09	30.81
	fcc	29.60	32.03	31.85
c	*top*	32.15	34.74	34.53
	Experiment	28.64[a]	30.49[a]	30.35[a]
	Theory (*normal*)	28.76[b]	30.17[b], 30.63[c]	30.29[c]
	normal	0.36	0.15	0.13
E_g	Experiment	0.35[d]	0.17[e],0.15[d], 0.13[f]	0.30[d], 0.21[f]
	Theory (*normal*)	0.30[g], 0.31[h]	0.08[h], 0.05[e]	0.03[e]
	normal	−4.30	−3.82	−3.17
E_{coh}	*fcc*	−4.00	−3.80	−3.16
	top	−3.98	−3.76	−3.04

[a]Reference [43].
[b]Reference [40].
[c]Reference [44].
[d]Reference [45].
[e]Reference [48].
[f]Reference [49].
[g]Reference [8].
[h]Reference [41].

slightly underestimated HSE06+SOC value [8,45,46]. We note that for Bi_2Se_3 GW corrections are known to change the character of the band gap from an indirect to a direct one [41,47].

B. Ultrathin V_2VI_3 nanofilms

1. *Energetics and thermodynamic stability of V_2VI_3 nanofilms*

For the nanofilms of these V_2VI_3 materials, we perform PBE+D2(+SOC) calculations to study their QL-QL interaction energy E^{QL} as well as to understand their electronic band properties as a function of increasing number of QLs, N^{QL}. Figure 2 shows the variation of E^{QL} for *normal*, *fcc*, and *top* structured nanofilms as a function of N^{QL} for Bi_2Se_3 [Fig. 2(a)], Bi_2Te_3 [Fig. 2(b)], and Sb_2Te_3 [Fig. 2(c)], respectively. E^{QL} for all three stackings considered in this work is calculated to be negative, and converge to the bulklike values (E^{QL}_{bulk}) with increasing N^{QL}. Taking the bulk-stacked *normal* structure as an example, we find that $E^{QL}_{bulk} = -0.41$, -0.61, and -0.51 eV for Bi_2Se_3, Bi_2Te_3, and Sb_2Te_3, respectively. The *top* structured nanofilms have the least favorable E^{QL}, while the naturally forming *normal* structure yields the most favorable E^{QL}, with almost similar values for *fcc* stacked

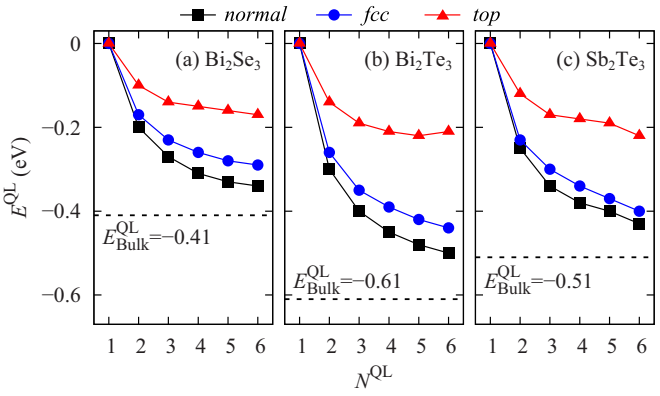

FIG. 2. (Color online) QL-QL interaction energy E^{QL} of *normal*, *fcc*, and *top* polymorphic nanofilms as a function of increasing number of QLs N^{QL} for (a) Bi_2Se_3, (b) Bi_2Te_3, and (c) Sb_2Te_3. As an example, the bulk limit of this interaction energy E^{QL}_{bulk} is shown as the horizontal dotted line for each V_2VI_3 compound.

nanofilms. These results are also consistent with the calculated cohesive energies of their bulk polymorphs, as illustrated above. Given that the calculated average difference in E^{QL} between the *normal* and *fcc* polymorphs is only about 0.06 eV, it is not difficult to imagine metastable *fcc* forming from *normal* stacked films via a martensitic-like (i.e., diffusionless) planar displacement, especially when the film thickness is in the nanometer range.

To study the energetic profile of this possible planar displacement, we use the the simplest 2 QL nanofilms for each V_2VI_3 to study planar displacement (here, we term this as *slippage*). Similar to the slippage in other two-dimensional materials, e.g., bilayer graphene and boron nitride [29,30], the upper QL may slip along the $\langle\bar{1}100\rangle$ or $\langle 1\bar{1}00\rangle$ directions as shown in Fig. 3(a). In these two directions, *normal*, *fcc*, and *top* structure will appear when the bottom Se atomic layer in the upper QL is located in B, C, and A sites, respectively. Since each QL is one unit, movement appears only between adjoining QLs. To understand the barrier needed to undergo this slippage in the $\langle\bar{1}100\rangle$ direction, we have also considered possible transition state (TS) structures between the *normal* and the *fcc* structured nanofilm. For the other $\langle 1\bar{1}00\rangle$ direction, the pathway goes via the *top* polymorph. These midway configurations are consistent with the slippage in bilayer graphene and boron nitride [50].

To calculate these slippage energy barriers, the energies of $E_1 (= E_{fcc} - E_{normal})$, $E_2 (= E_{TS} - E_{normal})$, and $E_3 (= E_{top} - E_{normal})$ have been defined in Fig. 3(a), where E_{normal}, E_{fcc}, E_{top}, and E_{TS} denote the energies of *normal*, *fcc*, and *top* structure as well as the transition state, respectively. As shown in Figs. 3(b)–3(d), the energies of *top* with respect to *normal* structured films, E_1 is calculated to be 0.049, 0.064, and 0.074 eV for Bi_2Se_3, Bi_2Te_3, and Sb_2Te_3, respectively. And based on our CI-NEB calculations, for the energy barrier in the $\langle\bar{1}100\rangle$ direction, E_2 is found to be 0.075, 0.108, and 0.117 eV for Bi_2Se_3, Bi_2Te_3, and Sb_2Te_3, respectively, while for the $\langle 1\bar{1}00\rangle$ direction, E_3 is found to be 0.205, 0.254, and 0.295 eV, correspondingly. We see that E_3 is at least two to three times larger than E_2 for all cases. Compared to the reported E^{QL} (19.3 meV) and area normalized E_2

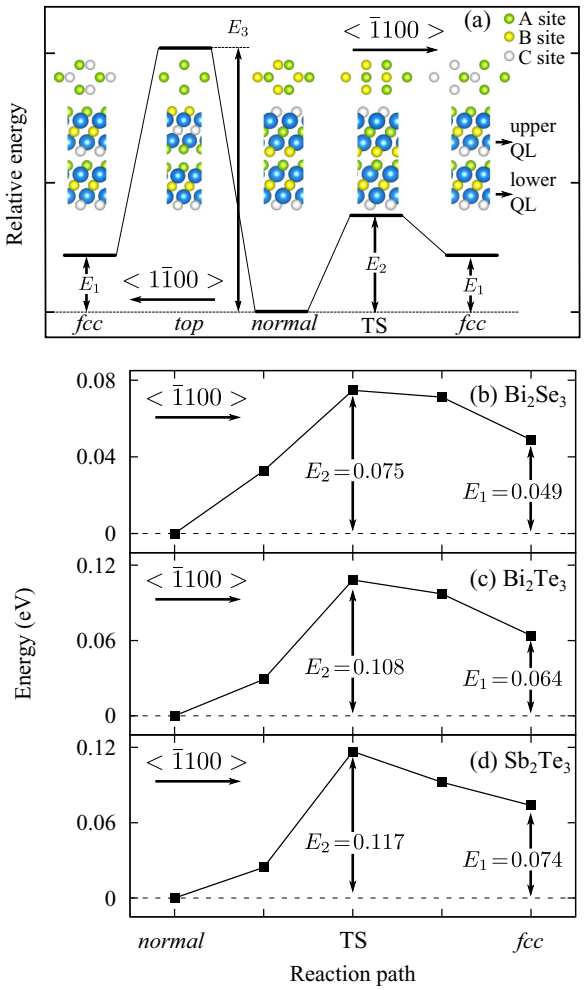

FIG. 3. (Color online) Energy profile for *slippage*: Relative energy differences between the *normal* and *fcc* structures for 2 QL nanofilms for two different paths, namely, along the $\langle \bar{1}100 \rangle$ (energy E_2) or $\langle 1\bar{1}00 \rangle$ (energy E_3) directions. Schematic energy profile along the $\langle \bar{1}100 \rangle$ direction for (b) Bi_2Se_3, (c) Bi_2Te_3, and (d) Sb_2Te_3. All energies are given with respect to the reference total energy of *normal* films.

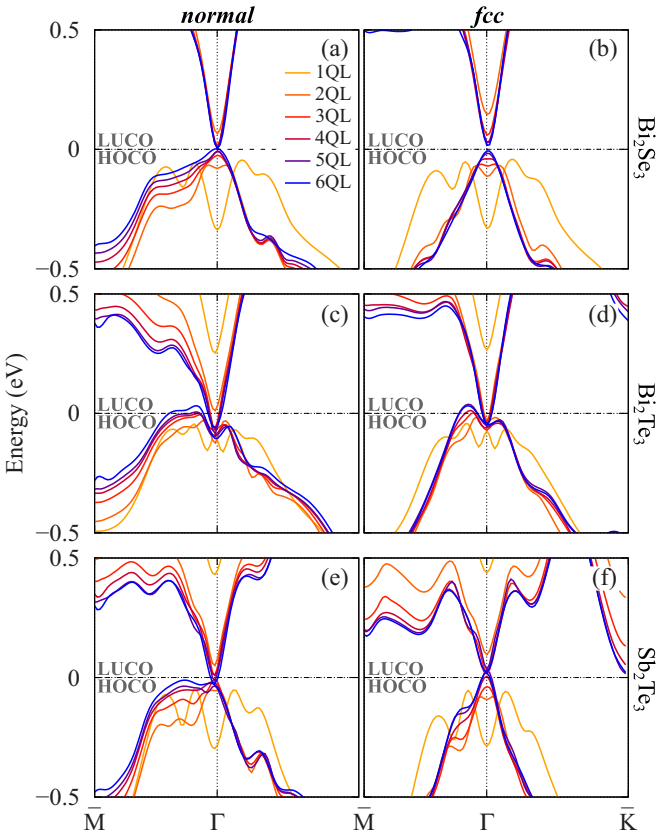

FIG. 4. (Color online) PBE+SOC DFT-derived QL-resolved electronic band structure of V_2VI_3 nanofilms (from 1 to 6 QL): (a) *normal* structure of Bi_2Se_3, (b) *fcc* structure of Bi_2Se_3, (c) *normal* structure of Bi_2Te_3, (d) *fcc* structure of Bi_2Te_3, (e) *normal* structure of Sb_2Te_3, and (f) *fcc* structure of Sb_2Te_3. Only the band edges due to the highest occupied crystal orbital (HOCO) and the lowest unoccupied crystal orbital (LUCO) are shown for clarity.

(1.6 meV/Å^2) values for bilayer graphene [29], we find rather similar orders of magnitude for the V_2VI_3 chalcogenide nanofilms: 13.8 and 4.8 meV/Å^2 for Bi_2Se_3 films, 18.3 and 5.5 meV/Å^2 for Bi_2Te_3 films, and 16.4 and 6.5 meV/Å^2 for Sb_2Te_3 films, respectively. This would then imply that the martensitic *normal*-to-*fcc* slippage would most probably occur for these V_2VI_3 chalcogenide nanofilms via the $\langle \bar{1}100 \rangle$ rather than the $\langle 1\bar{1}00 \rangle$ direction.

2. *Electronic structure of V_2VI_3 nanofilms*

Turning to the electronic structure of the *normal* and *fcc* stacked nanofilms of V_2VI_3, we study both the electronic band dispersion as well as the electron density plots (at the band edges) to understand how their topological insulating properties might be influenced by both stacking and film thickness in these nanosystems. In Fig. 4, we calculate and plot the electronic band structures (using PBE+SOC), showing only the highest occupied crystal orbital (HOCO) and the lowest unoccupied crystal orbital (LUCO) for different numbers of QLs. The full band structures are shown in Fig. 1 of the Supplemental Material [51], where the number of bands necessarily increases linearly with the thickness of the films. The overall band dispersion profile (especially near the Γ-point) of the *normal* structured films is found to be rather similar to those of the corresponding *fcc* polymorph, but the clear difference lies in the variation in the magnitude of E_g. To cross-check our PBE+SOC results, we have also selectively calculated the electronic structure of 1 and 2 QL *normal* and *fcc* stacking of Bi_2Se_3 using HSE06+SOC where the predicted E_g are plotted in Fig. 5.

For Bi_2Se_3, E_g decreases to zero when the N^{QL} of *normal* structured nanofilms increases to 6, while that of all *fcc*-like films remain greater than zero. The predicted E_g of Bi_2Se_3 *normal* structured films are in good agreement with other theoretical reports [22,24,40,41], but differ from the reported experimental data for Bi_2Se_3 films [21], as shown in Fig. 5(a). Interestingly, the predicted E_g of the *fcc* polymorphs, except for the 6 QL nanofilm, seem to agree closely with the experimental E_g of Bi_2Se_3 films. Accordingly, the predicted E_g of Bi_2Se_3 *fcc* structured films are systematically larger than that of the Bi_2Se_3 *normal* stacked. Our HSE06+SOC derived E_g for 2 QL *normal* and *fcc* structure show the same

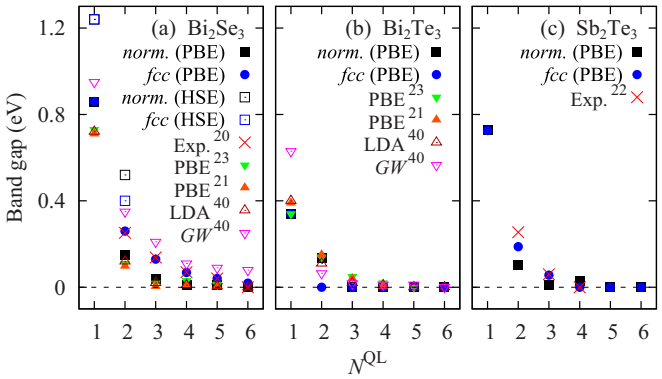

FIG. 5. (Color online) Γ-point band-gap energies E_g as a function of the number of QL, N^{QL}: (a) Bi_2Se_3, (b) Bi_2Te_3, and (c) Sb_2Te_3. *normal* (PBE) and *fcc* (PBE) denote the PBE+SOC value, while *normal* (HSE) and *fcc* (HSE) denote that calculated by the HSE06+SOC hybrid functional, respectively. The absolute values for these E_g are listed in Table I of the Supplemental Material [51].

tendency (albeit having larger absolute values of E_g, and poorer agreement with reported experimental values). The E_g of the *fcc* structured 6 QL is close to zero (0.02 eV), which may lead to a closure of the band gap when the N^{QL} increases continually. For Bi_2Te_3, as shown in Fig. 5(b), the E_g of the *normal* polymorph decreases to zero when N^{QL} is increased to 3, again agreeing with other theoretical reports [22,24,40,41]. In contrast to Bi_2Se_3, the E_g of the *fcc* structured films quickly reaches zero when N^{QL} reaches 2. For Sb_2Te_3, E_g of all *normal* structural films are greater than (or close to) zero for N^{QL} less than 5 while E_g decrease to zero when the N^{QL} of *fcc* stacked films increases to 4 [cf. Fig. 5(c)]. Again, the reported experimental data [23] seem to agree better with the predicted E_g of the *fcc* polymorph.

Based on the above comparison, within the accuracy of PBE+SOC DFT, the experimentally measured values of E_g for these V_2VI_3 nanofilms seem to better match those of V_2VI_3 *fcc* structured nanofilms, rather than the assumed more stable *normal* stacking. Although from our bulk calculations of Bi_2Se_3, we find that the PBE+SOC E_g value is found to agree better with available experimental and GW values, we cannot rule out the intrinsic deficiencies of semilocal DFT which could underestimate the predicted E_g values for these polymorphic nanofilms. We also note that a self-consistent relativistic quasiparticle treatment may change the quantitative nature of our results, but the qualitative trends discussed here are expected to be reliable.

Although vanishing values of E_g for some nanofilms are predicted, this is not sufficient information to conclude that these states are topologically protected. For systems with inversion symmetry, such as the V_2VI_3 compounds considered in this work, the Z_2 topological order can be determined by a parity analysis of the occupied states at time-reversal points in the Brillouin zone [5,41]. As a first approximation to this full Z_2 topological analysis [26], we plot and study the Γ-point electron density distributions (namely, the HOCO and LUCO states) for a selection of films in Fig. 6.

Taking the *normal* stacked 5 QL Bi_2Se_3 as a starting example, the HOCO state is more localized on the more

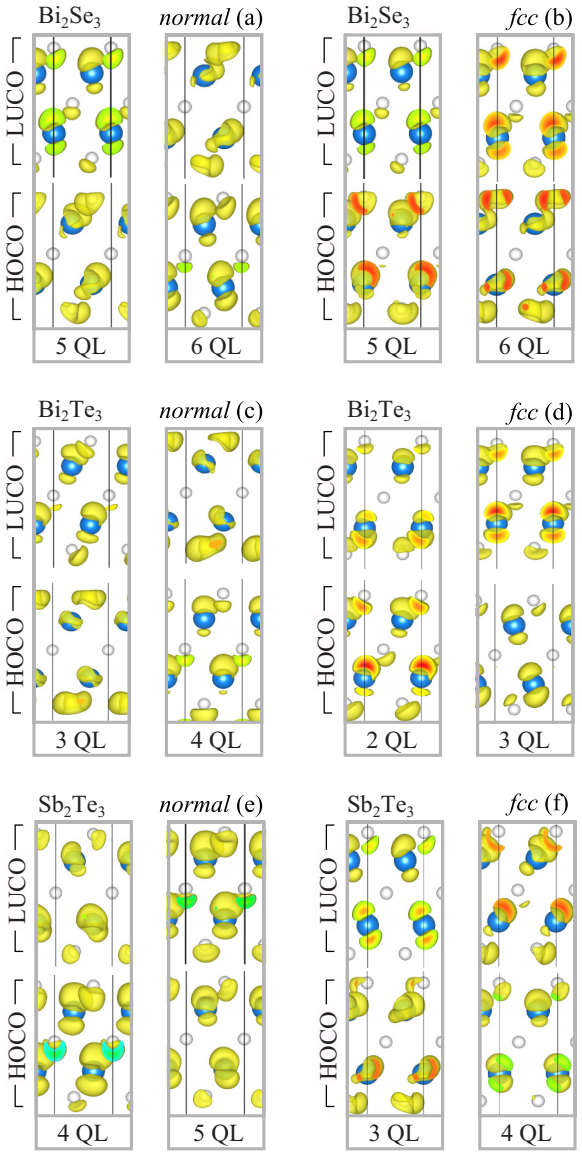

FIG. 6. (Color online) Γ-point electron density distributions (namely, the HOCO and LUCO states): (a) 5 and 6 QL *normal* structured films of Bi_2Se_3, (b) 5 and 6 QL *fcc* structured films of Bi_2Se_3, (c) 3 and 4 QL *normal* structured films of Bi_2Te_3, (d) 2 and 3 QL *fcc* structured films of Bi_2Te_3, (e) 3 and 4 QL *normal* structured films of Sb_2Te_3, and (f) 3 and 4 QL *fcc* structured films of Sb_2Te_3.

electronegative Se anion, while the electron density of the LUCO is mainly concentrated on the Bi cation, which is typical of a normal insulator. However, upon increasing N^{QL} to 6, the orbital symmetry of the HOCO and LUCO of the *normal* stacked 6 QL film inverts [as compared to that of 5 QL; see Fig. 6(a)]. The electron density plot of the 6 QL *normal* structured films LUCO resembles that of the HOCO of the 5 QL film, and vice versa. This inversion of the orbital character suggests a possible transition from a normal insulator (NI) to a TI, which has been observed in experimental measurements [21]. However, for the *fcc* stacked Bi_2Se_3 films, the calculated HOCO and LUCO plots for N^{QL} ranging from 1 to 6 show very similar orbital character, suggesting that no such NI to TI inversion has taken place. We illustrate this for the 5 and 6 QL

fcc structured films in Fig. 6(b). For the Bi_2Te_3 nanofilms, an orbital parity inversion is observed for both stackings *normal* and *fcc*, taking place at the increase from 3 QL to 4 QL for the *normal* structure [cf. Fig. 6(c)] and for the *fcc*-like films the inversion is observed when N^{QL} is increased from 2 to 3. Likewise, based on the electron density distribution for Sb_2Te_3, the orbital parity is predicted to be inverted for both, *normal* and *fcc* structure (i.e., 4 to 5 QL for *normal* and 3 to 4 QL for *fcc*). 1, the critical change from 3 to 4 QL in *fcc* structured films matches the experimental results better [23]. The inversion at a lower number of QLs for the *fcc* stacking may be due to a reduced overlap of the surface states since the *fcc* structured slabs are thicker than the *normal* stacked (cf. also Table I).

Upon studying the band gap E_g and orbital character inversion as a function of N^{QL} for the *normal* and *fcc* structure of these V_2VI_3 nanofilms, it seems to suggest that given the very low energy barriers for the *normal*-to-*fcc* slippage, metastable *fcc* structured nanofilms of these V_2VI_3 compounds could well form and offer different electronic band properties (e.g., critical N^{QL} for orbital parity inversion), especially for Bi_2Se_3 nanofilms. Thus, when these layered V_2VI_3 nanofilms are used in nanodevices, due to the weak interaction between these QLs, a mechanical slip could easily be experienced and thus the desired topological insulating character of these films could be intentionally exploited for new technologies.

III. CONCLUSION AND SUMMARY

The energetics of stacking sequences and their effect on the transition from normal to topological insulating behavior in Bi_2Se_3, Bi_2Te_3, and Sb_2Te_3 nanofilms have been investigated via first-principles DFT calculations. We find that the overall band dispersion is relatively insensitive to the stacking sequence, while the magnitude of the band gap, and the critical thickness for a band-edge parity inversion, is more sensitive. Relatively low energy barriers may allow for martensitic *normal*-to-*fcc* slippage, which are predicted to change the electronic structure and alter the topological behavior of these V_2VI_3 nanofilms. Thus, the effect of mechanical shear stress should be carefully considered in applications of topological insulators, e.g., the nanotribological conversion from TI to NI may be exploited in nanocircuit switches. In this context, a more detailed experimental analysis of the present and accessible stacking sequences is called for.

ACKNOWLEDGMENTS

The authors gratefully acknowledge support by the Global Frontier R & D Program (2013M3A6B1078881) on Center for Global Frontier Hybrid Interface Materials (GFHIM) funded by the Korean Ministry of Science, ICT & Future Planning, as well as the Australian Research Council (ARC). This work was also supported by the third Stage of Brain Korea 21 Plus Project Division of Creative Materials. Computational resources have been provided by the Australian National Computational Infrastructure (NCI) and by the KISTI supercomputing center (KSC-2013-C3-040). A.W. and B.Y. acknowledge support from the Royal Society University Research Fellowship scheme and the European Research Council Advanced Grant (No. ERC 291472), respectively.

[1] B. A. Bernevig, T. L. Hughes, and S.-C. Zhang, Science **314**, 1757 (2006).
[2] M. Z. Hasan and C. L. Kane, Rev. Mod. Phys. **82**, 3045 (2010).
[3] J. E. Moore, Nature (London) **464**, 194 (2010).
[4] X.-L. Qi and S.-C. Zhang, Rev. Mod. Phys. **83**, 1057 (2011).
[5] L. Fu and C. L. Kane, Phys. Rev. B **76**, 045302 (2007).
[6] D. Hsieh, D. Qian, L. Wray, Y. Xia, Y. S. Hor, R. J. Cava, and M. Z. Hasan, Nature (London) **452**, 970 (2008).
[7] B. Yan and S.-C. Zhang, Rep. Prog. Phys. **75**, 096501 (2012).
[8] H. Zhang, C.-X. Liu, X.-L. Qi, X. Dai, Z. Fang, and S.-C. Zhang, Nat. Phys. **5**, 438 (2009).
[9] G. Wang, X.-G. Zhu, Y.-Y. Sun, Y.-Y. Li, T. Zhang, J. Wen, X. Chen, K. He, L.-L. Wang, X.-C. Ma, J.-F. Jia, S. B. Zhang, and Q.-K. Xue, Adv. Mater. **23**, 2929 (2011).
[10] X. Chen, X.-C. Ma, K. He, J.-F. Jia, and Q.-K. Xue, Adv. Mater. **23**, 1162 (2011).
[11] D. O. Scanlon, P. D. C. King, R. P. Singh, A. de la Torre, S. McKeown Walker, G. Balakrishnan, F. Baumberger, and C. R. A. Catlow, Adv. Mater. **24**, 2154 (2012).
[12] S. Chadov, X. Qi, J. Kübler, G. H. Fecher, and C. Felser, Nat. Mater. **9**, 541 (2010).
[13] H. Lin, L. A. Wray, Y. Xia, S. Xu, S. Jia, R. J. Cava, A. Bansil, and M. Z. Hasan, Nat. Mater. **9**, 546 (2010).
[14] C. Li, J. S. Lian, and Q. Jiang, Phys. Rev. B **83**, 235125 (2011)
[15] H.-M. Guo and M. Franz, Phys. Rev. Lett. **103**, 206805 (2009).
[16] M. Dzero, K. Sun, V. Galitski, and P. Coleman, Phys. Rev. Lett. **104**, 106408 (2010).
[17] S. V. Eremeev, G. Bihlmayer, M. Vergniory, Y. M. Koroteev, T. V. Menshchikova, J. Henk, A. Ernst, and E. V. Chulkov, Phys. Rev. B **83**, 205129 (2011).
[18] H. Chen, W. Zhu, D. Xiao, and Z. Zhang, Phys. Rev. Lett. **107**, 056804 (2011).
[19] D. Kong and Y. Cui, Nat. Chem. **3**, 845 (2011).
[20] Y.-Y. Li, G. Wang, X.-G. Zhu, M.-H. Liu, C. Ye, X. Chen, Y.-Y. Wang, K. He, L.-L. Wang, X.-C. Ma, H.-J. Zhang, X. Dai, Z. Fang, X.-C. Xie, Y. Liu, X.-L. Qi, J.-F. Jia, S.-C. Zhang, and Q.-K. Xue, Adv. Mater. **22**, 4002 (2010).
[21] Y. Zhang, K. He, C.-Z. Chang, C.-L. Song, L.-L. Wang, X. Chen, J.-F. Jia, Z. Fang, X. Dai, W.-Y. Shan, S.-Q. Shen, Q. Niu, X.-L. Qi, S.-C. Zhang, X.-C. Ma, and Q.-K. Xue, Nat. Phys. **6**, 584 (2010).
[22] C.-X. Liu, H. J. Zhang, B. Yan, X.-L. Qi, T. Frauenheim, X. Dai, Z. Fang, and S.-C. Zhang, Phys. Rev. B **81**, 041307 (2010).
[23] Y. Jiang, Y. Wang, M. Chen, Z. Li, C. Song, K. He, L. Wang, X. Chen, X. Ma, and Q.-K. Xue, Phys. Rev. Lett. **108**, 016401 (2012).
[24] O. V. Yazyev, J. E. Moore, and S. G. Louie, Phys. Rev. Lett. **105**, 266806 (2010).

[25] K. Park, J. J. Heremans, V. W. Scarola, and D. Minic, Phys. Rev. Lett. **105**, 186801 (2010).
[26] W. Liu, X. Peng, C. Tang, L. Sun, K. Zhang, and J. Zhong, Phys. Rev. B **84**, 245105 (2011).
[27] S. M. Young, S. Chowdhury, E. J. Walter, E. J. Mele, C. L. Kane, and A. M. Rappe, Phys. Rev. B **84**, 085106 (2011).
[28] J. L. Zhang, S. J. Zhang, H. M. Weng, W. Zhang, L. X. Yang, Q. Q. Liu, S. M. Feng, X. C. Wang, R. C. Yu, L. Z. Cao, L. Wang, W. G. Yang, H. Z. Liu, W. Y. Zhao, S. C. Zhang, X. Dai, Z. Fang, and C. Q. Jin, Proc. Natl. Acad. Sci. USA **108**, 24 (2011).
[29] I. V. Lebedeva, A. A. Knizhnik, A. M. Popov, Y. E. Lozovik, and B. V. Potapkin, Phys. Chem. Chem. Phys. **13**, 5687 (2011).
[30] L. Liu, Y. P. Feng, and Z. X. Shen, Phys. Rev. B **68**, 104102 (2003).
[31] A. M. Popov, I. V. Lebedeva, A. A. Knizhnik, Y. E. Lozovik, and B. V. Potapkin, Phys. Rev. B **84**, 045404 (2011).
[32] G. Kresse and D. Joubert, Phys. Rev. B **59**, 1758 (1999).
[33] G. Kresse and J. Furthmüller, Phys. Rev. B **54**, 11169 (1996).
[34] J. P. Perdew, K. Burke, and M. Ernzerhof, Phys. Rev. Lett. **77**, 3865 (1996).
[35] T. J. Scheidemantel, C. Ambrosch-Draxl, T. Thonhauser, J. V. Badding, and J. O. Sofo, Phys. Rev. B **68**, 125210 (2003).
[36] S. Grimme, J. Antony, S. Ehrlich, and H. Krieg, J. Chem. Phys. **132**, 154104 (2010).
[37] Grimme's DFT-D3 program, URL: *http://toc.uni-muenster.de/DFTD3*
[38] C. Franchini, V. Bayer, R. Podloucky, J. Paier, and G. Kresse, Phys. Rev. B **72**, 045132 (2005).
[39] A. V. Krukau, O. A. Vydrov, A. F. Izmaylov, and G. E. Scuseria, J. Chem. Phys. **125**, 224106 (2006).
[40] X. Luo, M. B. Sullivan, and S. Y. Quek, Phys. Rev. B **86**, 184111 (2012).
[41] O. V. Yazyev, E. Kioupakis, J. E. Moore, and S. G. Louie, Phys. Rev. B **85**, 161101 (2012).
[42] G. Henkelman, B. P. Uberuaga, and H. Jónsson, J. Chem. Phys. **113**, 9901 (2000).
[43] *Crystal Structures Volume 2*, edited by R. W. G. Wyckoff (Wiley, New York, 1964).
[44] G. Wang and T. Cagin, Phys. Rev. B **76**, 075201 (2007).
[45] J. Black, E. M. Conwell, L. Seigle, and C. W. Spencer, J. Phys. Chem. Solids **2**, 240 (1957).
[46] J. Vidal, X. Zhang, L. Yu, J.-W. Luo, and A. Zunger, Phys. Rev. B **84**, 041109 (2011).
[47] I. A. Nechaev, R. C. Hatch, M. Bianchi, D. Guan, C. Friedrich, I. Aguilera, J. L. Mi, B. B. Iversen, S. Blügel, P. Hofmann, and E. V. Chulkov, Phys. Rev. B **87**, 121111 (2013).
[48] Y. L. Chen, J. G. Analytis, J.-H. Chu, Z. K. Liu, S.-K. Mo, X. L. Qi, H. J. Zhang, D. H. Lu, X. Dai, Z. Fang, S. C. Zhang, I. R. Fisher, Z. Hussain, and Z.-X. Shen, Science **325**, 178 (2009).
[49] R. Sehr and L. R. Testardi, J. Phys. Chem. Solids **23**, 1219 (1962).
[50] Y. Sakamoto, T. Hirahara, H. Miyazaki, S.-i. Kimura, and S. Hasegawa, Phys. Rev. B **81**, 165432 (2010).
[51] See Supplemental Material at http://link.aps.org/supplemental/10.1103/PhysRevB.90.075438 for more details on the electronic band structures and band-gap energies as a function of N^{QL}.